Chemical Science

ROYAL SOCIETY OF CHEMISTRY

EDGE ARTICLE

View Article Online
View Journal | View Issue

Cite this: *Chem. Sci.*, 2022, **13**, 3027

All publication charges for this article have been paid for by the Royal Society of Chemistry

Received 26th November 2021
Accepted 15th February 2022

DOI: 10.1039/d1sc06596c

rsc.li/chemical-science

Selective covalent targeting of SARS-CoV-2 main protease by enantiopure chlorofluoroacetamide†

Daiki Yamane,[a] Satsuki Onitsuka,[a] Suyong Re,[b] Hikaru Isogai,[a] Rui Hamada,[a] Tadanari Hiramoto,[a] Eiji Kawanishi,[a] Kenji Mizuguchi,[bc] Naoya Shindo *[a] and Akio Ojida *[a]

The coronavirus disease 2019 (COVID-19) pandemic has necessitated the development of antiviral agents against severe acute respiratory syndrome coronavirus 2 (SARS-CoV-2). The main protease (M^{pro}) is a promising target for COVID-19 treatment. Here, we report an irreversible SARS-CoV-2 M^{pro} inhibitor possessing chlorofluoroacetamide (CFA) as a warhead for the covalent modification of M^{pro}. Ugi multicomponent reaction using chlorofluoroacetic acid enabled the rapid synthesis of dipeptidic CFA derivatives that identified **18** as a potent inhibitor of SARS-CoV-2 M^{pro}. Among the four stereoisomers, (*R*,*R*)-**18** exhibited a markedly higher inhibitory activity against M^{pro} than the other isomers. Reaction kinetics and computational docking studies suggest that the *R* configuration of the CFA warhead is crucial for the rapid covalent inhibition of M^{pro}. Our findings highlight the prominent influence of the CFA chirality on the covalent modification of proteinous cysteines and provide the basis for improving the potency and selectivity of CFA-based covalent inhibitors.

Introduction

The outbreak of the novel coronavirus disease 2019 (COVID-19), caused by severe acute respiratory syndrome coronavirus 2 (SARS-CoV-2),[1,2] poses a severe threat to global public health and economy. Although efficacious vaccines are now being administered worldwide, novel SARS-CoV-2 variants of interest and concern continue to emerge.[3] Thus, the development of antiviral agents against SARS-CoV-2 is urgently needed to tackle and end the current pandemic.[4,5] SARS-CoV-2 has a single-stranded genomic RNA that encodes polyproteins pp1a and pp1ab. Two cysteine proteases, the main protease (M^{pro}, also known as 3C-like protease, $3CL^{pro}$) and the papain-like protease (PL^{pro}), are excised from these polyproteins and further digest the polyproteins into nonstructural proteins, including crucial components of the viral replication–translation machinery. Although both proteases are essential for viral replication, the predominant role of M^{pro} in polyprotein processing and the lack of a human homolog has led to extensive studies to establish it as an attractive drug target against SARS-CoV-2.[6,7]

M^{pro} recognizes glutamine and a hydrophobic amino acid residue at the S1 and S2 pockets in the active site, respectively, and cleaves amide bonds primarily within the Leu-Gln↓(Ser, Ala, Gly) sequence (↓: cleavage site).[8] This substrate specificity is conserved across other coronaviruses, including SARS-CoV-1 and middle east respiratory syndrome coronavirus (MERS-CoV).[9,10] Therefore, current efforts to develop SARS-CoV-2 M^{pro} inhibitors are extensively guided by the previous molecular designs, especially those targeting SARS-CoV-1 M^{pro}.[5,6] Most of the reported SARS-CoV-2 M^{pro} inhibitors are peptidomimetics based on the Leu-Gln sequence, combined with an electrophilic warhead, such as α-ketoamide,[11] aldehyde,[12–15] ketone,[16–19] vinyl sulfone,[8] and nitrile,[20,21] for the covalent capture of the sulfhydryl group of the catalytic Cys145. Nirmatrelvir (PF-07321332), developed by Pfizer, is one of the most advanced compounds in this category and has been recently approved by regulatory ageincies as a combination with ritonavir (Fig. 1A).[21] Other than peptidomimetics, several Ugi multicomponent reaction (MCR)-generated dipeptidic compounds have been reported as inhibitors against SARS-CoV-1 and SARS-CoV-2 M^{pro} (Fig. 1B).[22–24]

Covalent inhibition of proteins has been a powerful strategy for achieving potent and sustained pharmacological efficacy.[25] To date, a number of acrylamide-based covalent inhibitors targeting a noncatalytic cysteine of proteins have been clinically approved or under clinical trials for cancer treatment.[26,27] In development of covalent inhibitors, high target selectivity should be ensured to minimize the risk of toxicity due to off-

[a]*Graduate School of Pharmaceutical Sciences, Kyushu University, 3-1-1 Maidashi, Higashi-ku, Fukuoka 812-8582, Japan. E-mail: shindo708@phar.kyushu-u.ac.jp; ojida@phar.kyushu-u.ac.jp*

[b]*Artificial Intelligence Center for Health and Biomedical Research, National Institute of Biomedical Innovation, Health and Nutrition, 7-6-8 Saito-Asagi, Ibaraki, Osaka 567-0085, Japan*

[c]*Institute for Protein Research, Osaka University, 3-2 Yamadaoka, Suita, Osaka 565-0871, Japan*

† Electronic supplementary information (ESI) available: Supplemental figures, experimental methods, and synthetic procedures. CCDC 2124399 and 2124400. For ESI and crystallographic data in CIF or other electronic format see DOI: 10.1039/d1sc06596c

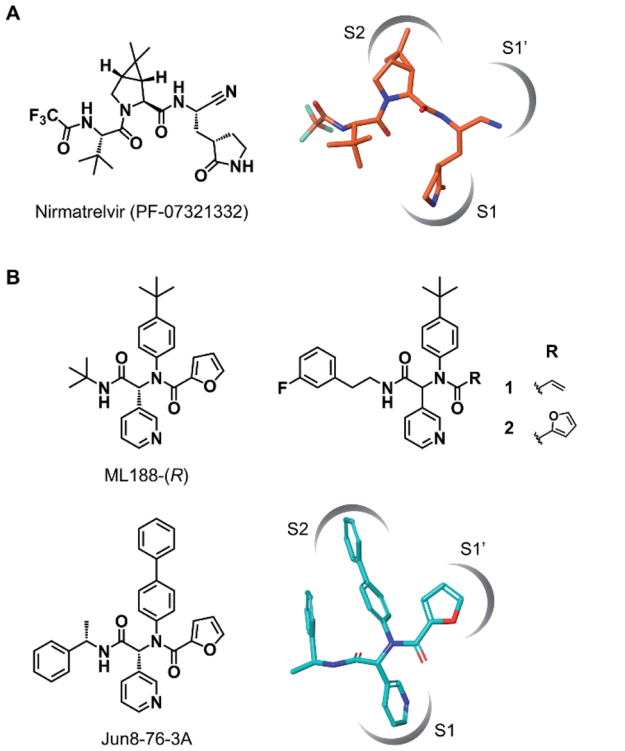

Fig. 1 Chemical structures of SARS-CoV-2 M^{pro} inhibitors. (A) Structure of nirmatrelvir (PF-07321332) and its binding mode in the M^{pro} active site (the conformation was retrieved from the cocrystal structure, PDB code 7RFW). (B) The structures of dipeptidic M^{pro} inhibitors generated by Ugi multicomponent reaction and the binding mode of Jun8-76-3A in the M^{pro} active site (the conformation was retrieved from the cocrystal structure, PDB code 7KX5).

target labeling.[28] This point is also crucial for designing covalent inhibitors targeting SARS-CoV-2 M^{pro}, as medications for infectious diseases generally require a broader safety margin than cancer treatment. We have recently introduced α-chlorofluoroacetamide (CFA) as a weakly reactive, cysteine-directed warhead for covalent inhibition of proteins including tyrosine kinases.[29–31] We found that the CFA derivatives exhibited higher selectivity in covalent modification toward the targeted tyrosine kinases than the structurally related acrylamide-based inhibitors. We also demonstrated that the CFA–thiol adduct is hydrolyzed under neutral aqueous conditions to reversibly generate an unmodified cysteine, which could contribute to high target selectivity by eliminating the solvent-exposed off-target labeling. These desirable features led us to envision CFA as a valuable tool for designing selective covalent SARS-CoV-2 M^{pro} inhibitors.

Results and discussion

Wang *et al.* recently reported Jun8-76-3A as a reversible inhibitor of SARS-CoV-2 M^{pro}.[23] The molecular architecture of Jun8-76-3A is based on ML188-(*R*) that was previously developed as an inhibitor of SARS-CoV-1 M^{pro}.[22] The crystal X-ray structure analysis revealed that the 3-pyridyl group of Jun8-76-3A resides in the S1 glutamine binding pocket of SARS-CoV-2 M^{pro} by forming a hydrogen bond with His163. The 4-biphenyl group occupies the S2 pocket that prefers hydrophobic amino acid residues like leucine and phenylalanine. The furan-2-carboxamide moiety exerts a bifurcated interaction with the backbone NH of Gly143 in the S1′ pocket, wherein the catalytic Cys145 resides. Based on the same Ugi MCR-generated dipeptide scaffold, London *et al.* reported an acrylamide-based covalent SARS-CoV-2 M^{pro} inhibitor **1**.[24] We also employed this dipeptide scaffold as the starting point for the development of a CFA-based covalent inhibitor against M^{pro}. Ugi MCR using racemic chlorofluoroacetic acid, along with amine, aldehyde, and isocyanide, proceeded smoothly to yield CFA compound **3** as a mixture of diastereomers in a single step. The two diastereomers, **3A** (less polar isomer) and **3B** (more polar isomer), were separable by silica gel chromatography (Fig. 2A). The inhibitory activity of these compounds was assessed by an enzymatic assay using the recombinant SARS-CoV-2 M^{pro} and the fluorogenic substrate Ac-Abu-Tle-Leu-Gln-(4-methyl-coumaryl-7-amide).[8] This substrate allowed robust fluorescent reading compared to the FRET-based substrate possessing an Edans/Dabcyl donor–acceptor pair.[32] We found that **3A** and **3B** displayed different inhibitory activities against M^{pro} (Fig. 2B); **3B** exhibited moderate inhibitory activity (IC_{50} = 1.05 μM), whereas **3A** was virtually inactive (IC_{50} > 20 μM). In the case of ML188 and Jun8-76-3A, it has been reported that the *R* configuration of the pyridyl α-carbon is crucial for M^{pro} inhibition.[22,23] Considering that both **3A** and **3B** contain the *R* configuration at this stereocenter, our results suggest that the chirality at the CFA stereocenter also substantially impacts their inhibitory activities. Non-reactive analogs of **3** such as acetamide **4** and

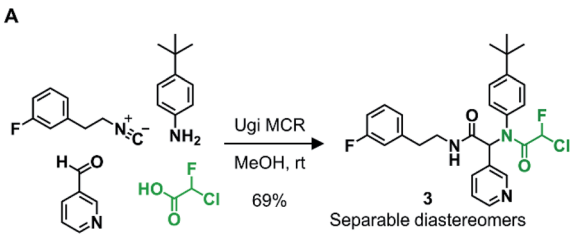

Compound	IC_{50} (μM)
Jun8-76-3A	0.95 ± 0.035
1	2.62 ± 0.097
2	2.68 ± 0.092
3A	> 20
3B	1.05 ± 0.079
4	> 20
5	> 20

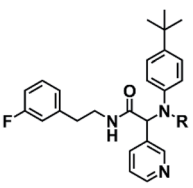

Fig. 2 (A) Preparation of the dipeptidic inhibitor **3** *via* Ugi multicomponent reaction (MCR). (B) Enzyme inhibitory activities of the dipeptidic inhibitors against SARS-CoV-2 M^{pro}. Compounds **3A** and **3B** are the less and more polar diastereomers, respectively. The reported IC_{50} values for Jun8-76-3A, **1**, and **2** are 0.31, 2.95, and 2.72 μM, respectively.

difluoroacetamide **5** were found to be inactive (IC_{50} > 20 μM), indicating that the covalent attachment at CFA contributes to the M^{pro} inhibitory activity of **3B** in a stereospecific manner. In the same assay, we also found that acrylamide **1** showed a weaker activity (IC_{50} = 2.62 μM) than **3B**.

This observation encouraged us to subsequently conduct an SAR study to improve the potency of CFA dipeptides (Fig. 3A). We first evaluated the effect of the *para*-substituent of the benzene ring (R^1) on inhibitory activity. As this moiety occupies the S2 pocket that primarily accommodates a leucine residue, we screened compounds **6–9** with a hydrophobic *para*-substituent. In the assay, less polar diastereomer A was inactive (IC_{50} > 20 μM), whereas more polar diastereomer B showed moderate activity in all the cases. Among them, **9B** possessing a pentafluorosulfanyl (SF_5) group, a thermally and chemically stable bioisostere for a *tert*-butyl group,[33] exhibited a slightly higher M^{pro} inhibitory activity (IC_{50} = 0.90 μM) than **3B**. Next, we investigated the effect of the heteroaromatic ring (R^2) on the activity. The replacement of the pyridine ring of **3B** with a diazine increased the potency of **11–12**, whereas the 3-pyridazinyl derivative **10** was almost inactive (IC_{50} > 20 μM as a diastereomixture). 5-Pyrimidine **12** was the only compound with separable diastereomers, and **12B** exhibited the highest activity in the series (IC_{50} = 0.25 μM). The effect of the substituent R^3 was also investigated. The introduction of a *tert*-butyl group, as observed in the structure of ML188, reduced the potency (**14B**, IC_{50} = 2.70 μM). Replacement of the 3-fluorophenyl group of **3** to a 3-pyridyl group slightly increased the activity (**16**, IC_{50} = 0.73 μM as a diastereomixture). The introduction of a 7-isoquinoline ring resulted in a slight loss of activity (**17B**, IC_{50} = 1.43 μM). Combining the SAR results, we synthesized compound **18** and **19** as structurally optimized CFA inhibitors (Fig. 3B). The diastereomers were separable in both cases and the active isomers **18B** and **19B** exhibited potent M^{pro} inhibitory activities (IC_{50} = 0.21 and 0.14 μM, respectively). Although **19B** was marginally more active than **18B**, we chose **18** for further investigations because the chromatograhic separation of the diastereomixture of **18** was much easier than that of **19**. Fortunately, we were able to determine the relative configuration of **18B** by X-ray crystallography (Fig. S1†). The analyzed structure revealed that **18B** has a *syn*-configuration, where the 5-pyrimidinyl group and the CFA fluorine atom are oriented toward the same direction in the drawn structure (Fig. 3C). Consequently, **18A** was determined to be an *anti*-isomer.

To elucidate the relationship between the CFA chirality and the inhibitory activity, we next attempted to obtain the four stereoisomers of **18** in enantiomerically pure form using optically active chlorofluoroacetic acid.[34] Wakselman previously reported the preparation of optically active chlorofluoroacetyl chloride based on the chromatographic separation of the

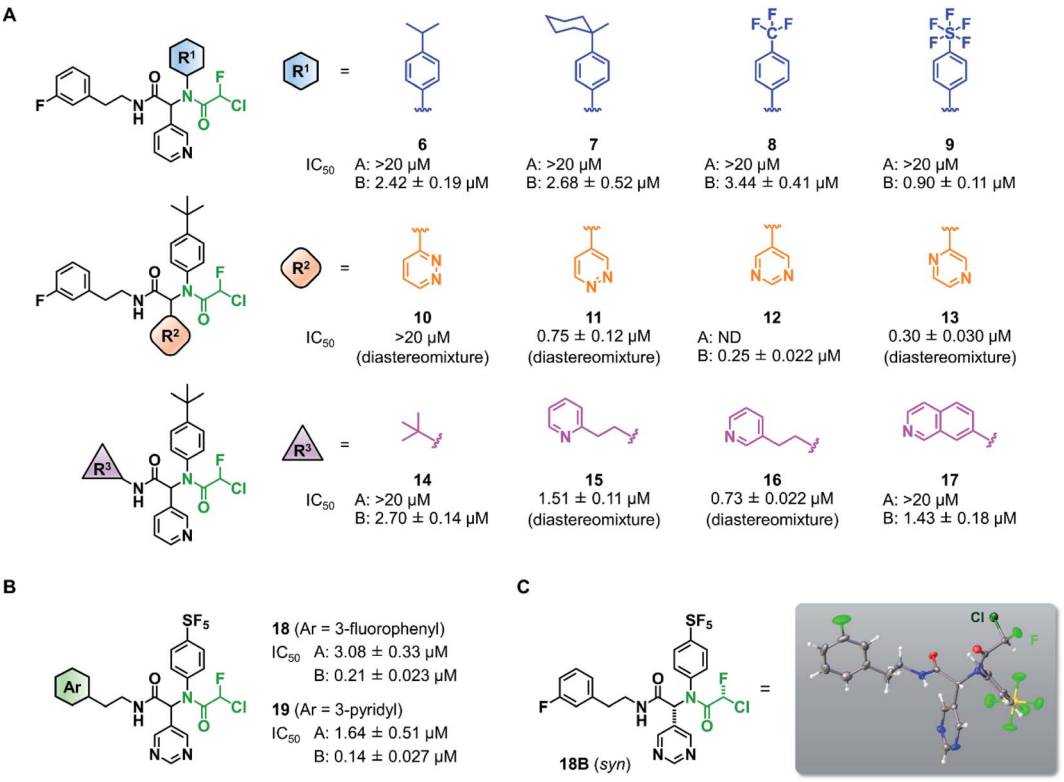

Fig. 3 Structure–activity relationship of chlorofluoroacetamide (CFA) derivatives. (A) Screening of the CFA derivatives with the different R^1, R^2, and R^3 substituents. ND, not determined. A and B indicate the less and more polar diastereomers separated by silica gel column chromatography. (B) The structures and inhibitory activities of the CFA dipeptides **18** and **19**. (C) The relative configuration of **18B** determined by X-ray crystallography (see Fig. S1†).

diastereomers of CFA **20** derived from (*S*)-(−)-1-phenethylamine.[35] However, the isolation of diastereomers of **20** proved to be laborious in our attempts due to poor separation by silica gel chromatography. Thus, we established a new method employing (*R*)-(−)-2-phenylglycinol as a chiral resolving agent (Scheme 1). We found that the diastereomers of CFA **21**, readily accessible from commercially available (*R*)-(−)-2-phenylglycinol and ethyl chlorofluoroacetate, were easily separated by silica gel chromatography and afforded pure **21A** and **21B** on a multigram scale. X-ray crystallography determined the absolute configuration at the CFA chiral center to be *R* in **21B** (Fig. S2†). Isolated **21A** and **21B** were subjected to hydrolysis in refluxing 3 M H_2SO_4/1,4-dioxane to afford (*S*)- and (*R*)-chlorofluoroacetic acid, respectively. Finally, Ugi MCR using enantiopure chlorofluoroacetic acids and subsequent chromatographic separation of the diastereomers yielded a set of four stereoisomers of **18**.

Having the four stereoisomers of **18** in hand, we evaluated their inhibitory activities against SARS-CoV-2 M^{pro} (Fig. 4). We found that (*R*,*R*)-**18** (the former *R* indicates the absolute configuration at the Ugi MCR-generated stereocenter, and the latter at CFA) exclusively exhibited strong activity (IC_{50} = 0.056 μM) among the four stereoisomers (Fig. 4B and D). Notably, this activity is much higher than that of (*R*,*S*)-**18** possessing an (*S*)-CFA warhead (IC_{50} = 10.62 μM), indicating that the chirality at CFA greatly influences the inhibitory activity. The IC_{50} values of the other isomers (*S*,*R*)-**18** and (*S*,*S*)-**18** were 2.24 and 14.04 μM, respectively. To further investigate these results, we performed a kinetic analysis of M^{pro} inhibition by (*R*,*R*)-**18** and its diastereomers (*S*,*R*)- and (*R*,*S*)-**18**.[36] All three isomers inhibited the hydrolysis of the fluorogenic substrate by M^{pro} in a time-dependent manner, indicating an irreversible mode of action (Fig. 4C and S3–S5†). The kinetic parameters for irreversible inactivation of M^{pro} are summarized in Fig. 4D. As expected, the most potent isomer (*R*,*R*)-**18** inactivated M^{pro} with much higher efficiency (k_{inact}/K_I = 4167 M^{-1} s^{-1}) than the diastereomers (*S*,*R*)- and (*R*,*S*)-**18** (k_{inact}/K_I = 66.0 and 20.0 M^{-1} s^{-1}, respectively). (*R*,*R*)-**18** exhibited both a higher k_{inact} value and a lower K_I value than those of (*R*,*S*)-**18**, suggesting that the CFA chirality largely affected the reaction rate of covalent modification as well as the binding affinity with M^{pro}. In comparison between (*R*,*R*)-**18** and (*S*,*R*)-**18**, the binding constant K_I was significantly different (1.34 and 64.7 μM, respectively), whereas the inactivation rates were similar (k_{inact} = 0.0056 and 0.0043 s^{-1}, respectively). This marked difference in K_I value was consistent with previous studies of ML188 and Jun8-76-3A, where the *R* configuration at the α-pyridine chiral center was crucial for the inhibitory activities.[22,23] We also determined the kinetic parameters of acrylamide **1** (Fig. S6†). Despite higher thiol reactivity of acrylamide than CFA,[29] the k_{inact} value of **1** was significantly smaller than (*R*)-CFA. This result implies the mismatched disposition of the acrylamide warhead in the **1**–M^{pro} binding complex for the Michael addition of the thiol group of Cys145.

To gain further insight into the effect of CFA chirality, we performed docking simulations of the stereoisomers of **18** against M^{pro}. Based on the X-ray cocrystal structure of (*R*)-**1** with SARS-CoV-2 M^{pro} (PDB code 7NW2),[24] we examined the possible binding poses and affinities of each of the four isomers, (*R*,*R*)-, (*R*,*S*)-, (*S*,*R*)-, and (*S*,*S*)-**18** in the same pocket of M^{pro}. The predicted binding affinities for the stereoisomers fell into the range of 2 kcal mol^{-1} difference, but there found no clear correlation with the experimental result. To find out the cause of the higher reactivity of (*R*,*R*)-**18**, we assessed the occurrences of "reactive conformations" in the predicted poses for the four isomers, where we defined the pose as reactive for the S_N2 reaction (backside attack of Cys145 to the CFA carbon) if the C···S distance <4.5 Å and Cl–C···S angle >150°. We found a large number of reactive conformations (46 out of 183 poses) exclusively in the low binding energy region for (*R*,*R*)-**18** among the four stereoisomers (Fig. S7†). The most stable pose of (*R*,*R*)-**18** was S_N2-reactive, where the Cl–C···S angle is nearly 180° (Fig. 4E). In the complex, the CFA fluorine and the carbonyl oxygen were close proximity to the backbone NH of Gly143, which is thought to constitute the oxyanion hole in the S1′ pocket.[37] This result suggests the potential contribution of NH···F hydrogen bond to facilitate the reaction. The bound structure of (*R*,*R*)-**18** was well aligned to the X-ray crystal structure of a dichloroacetamide inhibitor Jun9-62-2R covalently bound to M^{pro}, which was recently reported by Wang *et al.* (Fig. S8†).[38] On the other hand, the most stable pose of (*R*,*S*)-**18** was S_N2-non-reactive due to the unpreferable orientation of the C–Cl bond for the nucleophilic attack by Cys145. The rotation of the CFA unit of (*R*,*S*)-**18** could give an S_N2-reactive pose, but the resulting rotamer lacks any stabilizing interaction with the M^{pro} active site. Taken together, we infer that (*R*,*R*)-**18** is more likely to become S_N2-reactive as the NH···F hydrogen bond forces the C–Cl bond to a favorable orientation in the binding complex. The NH···F hydrogen bond in the (*R*,*R*)-**18**–M^{pro} complex could also contribute to increasing the electrophilic reactivity of the CFA warhead.

The inhibitory activity of (*R*,*R*)-**18** against other cysteine proteases was evaluated (Fig. 5A). (*R*,*R*)-**18** potently inhibited SARS-CoV-1 M^{pro} with an IC_{50} value of 0.094 μM. This result was not surprising because the structures of M^{pro} are highly conserved between SARS-CoV-1 and SARS-CoV-2 (96% identity of the amino acid sequence). (*R*,*R*)-**18** did not inhibit SARS-CoV-2 papain-like protease (PL^{pro}) (<1% inhibition at 20 μM). Human cathepsin B and L were not inhibited by 20 μM of (*R*,*R*)-**18**, whereas the noncovalent inhibitor Jun8-76-3A weakly

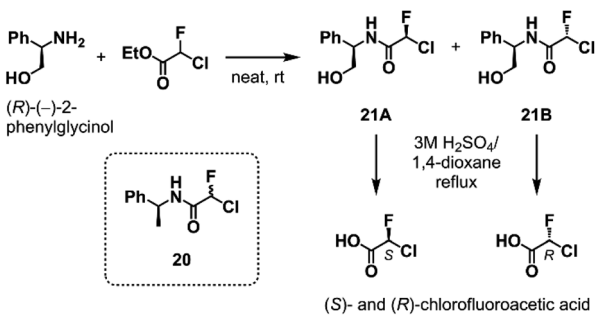

Scheme 1 The optical resolution of chlorofluoroacetic acid using (*R*)-(−)-2-phenylglycinol as a chiral resolving agent. See ESI† for the detail.

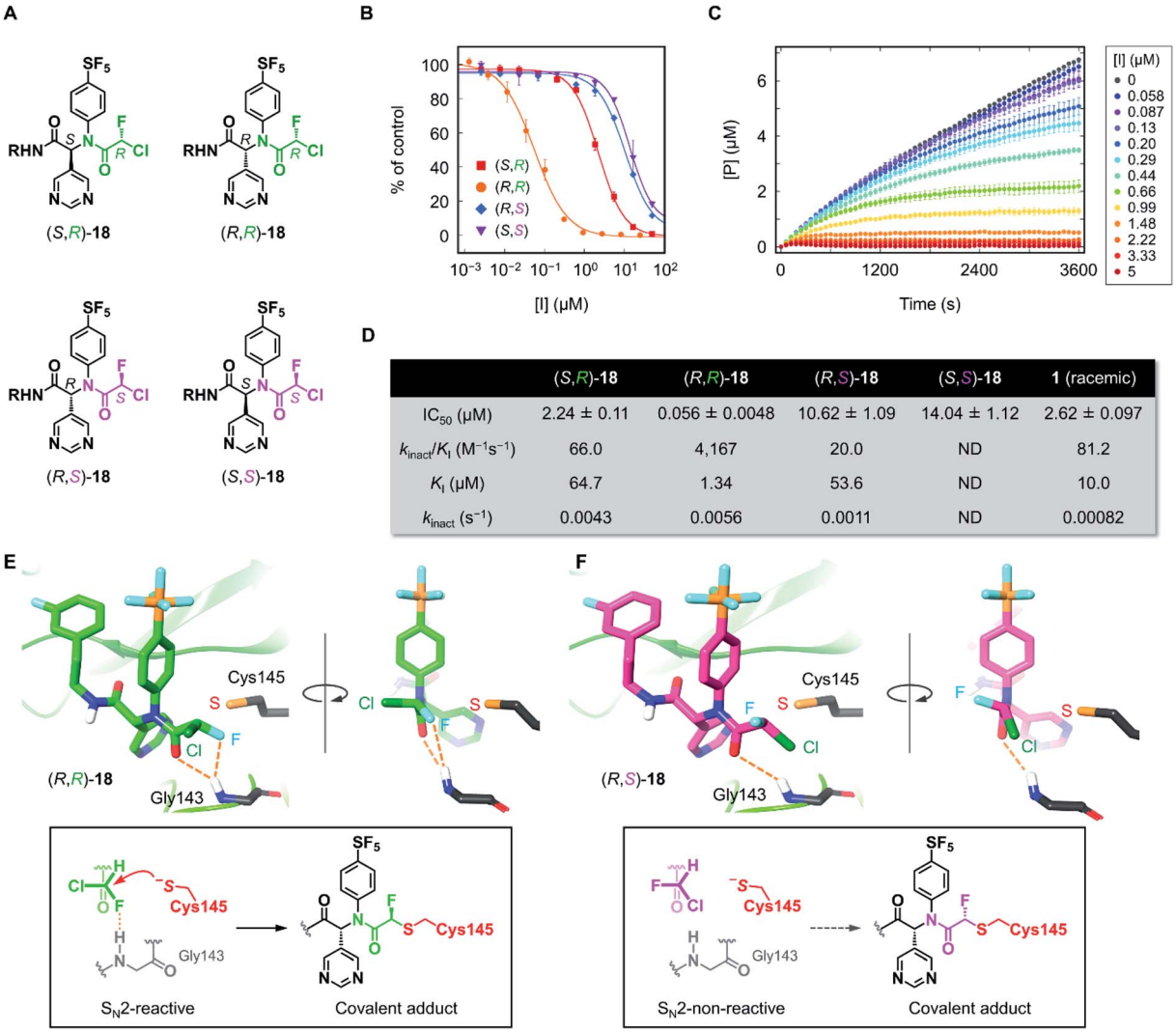

Fig. 4 Inhibition properties of the four stereoisomers of **18** against SARS-CoV-2 M^{pro}. (A) The absolute configurations of the stereoisomers of **18** (R = (3-fluorophenyl)ethyl). The *R* and *S* configurations at the CFA unit are highlighted in green and magenta, respectively. (B) The inhibitory activity of the stereoisomers against SARS-CoV-2 M^{pro}. Each plot represents the mean of triplicate experiments ± standard deviation. (C) Time-course plot of the M^{pro}-catalyzed hydrolysis of the fluorogenic substrate in the presence of various concentrations of (*R*,*R*)-**18**. [P] represents the concentration of the hydrolyzed product of the fluorogenic peptide substrate determined by the fluorescence intensity. Each plot represents the mean of triplicate experiments ± standard error of the mean. (D) Summary of IC_{50} values and kinetic parameters of the chiral stereoisomers of **18**. ND, not determined. (E) and (F) The computationally predicted, most stable conformations of (*R*,*R*)- and (*R*,*S*)-**18** in the M^{pro} active site. See ESI† for a detailed computational method.

inhibited cathepsin B (55% inhibition at 20 μM). To assess the covalent binding properties of the CFA inhibitor, we designed a clickable activity-based probe (*R*,*R*)-**22** (Fig. 5B). Introduction of the ethynyl group was well tolerated, and (*R*,*R*)-**22** exhibited potent inhibitory activity against SARS-CoV-2 M^{pro} (IC_{50} = 0.11 μM) comparable to that of (*R*,*R*)-**18** (IC_{50} = 0.056 μM). In the gel-based *in vitro* assay, the recombinant SARS-CoV-2 M^{pro} was treated with (*R*,*R*)-**22** (37 °C, 1 h) and conjugated to rhodamine-azide by copper-catalyzed azide–alkyne cycloaddition (CuAAC). The in-gel fluorescence analysis showed that M^{pro} could be detected at concentrations as low as 10 nM by 2.5 μM of (*R*,*R*)-**22**, and 50 nM of M^{pro} was labeled by (*R*,*R*)-**22** in a concentration-dependent manner (0.1–10 μM). Incubation of (*R*,*R*)-**22** with A431 cell lysate spiked with M^{pro} (50 nM) showed the main band at ~34 kDa. This band disappeared after preincubation with the covalent inhibitors PF-00835231 (ref. 16) and (*R*,*R*)-**18** (5 μM, 30 min), but not with the reversible inhibitor Jun8-76-3A (Fig. 5C and S9†). These results demonstrate the ability of the CFA-type inhibitor to covalently modify M^{pro} in the complex human proteome. We also synthesized acrylamide probe **23** as an alkynylated analog of **1** and evaluated its proteome-wide activity under live cell conditions (Fig. 5D and S10†). Treatment of A431 cells with (*R*,*R*)-**22** or **23** (1–10 μM, 37 °C, 1 h) and the subsequent in-gel fluorescence analysis revealed that acrylamide **23** exhibited a higher level of off-target labeling compared to **22**, suggesting a low indiscriminate reactivity of the dipeptidic CFA inhibitor in live cells.

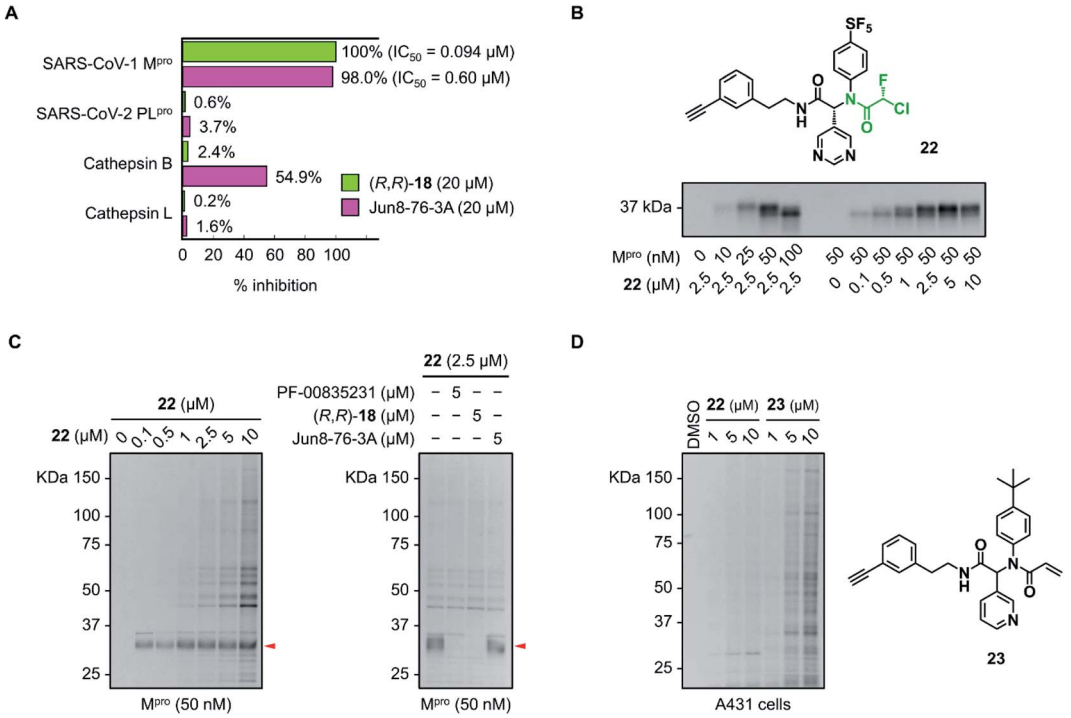

Fig. 5 Selectivity profiles of the CFA inhibitors toward SARS-CoV-2 M^{pro}. (A) Inhibitory activity of (*R*,*R*)-**18** and Jun8-76-3A toward the different cysteine proteases. The data are represented as the average of two independent experiments. (B) In-gel fluorescence analysis of the labeling of the recombinant M^{pro} with CFA probe **22** (37 °C, 1 h). (C) Reactivity profiles of (*R*,*R*)-**22** toward the M^{pro} spiked into A431 cell lysate (37 °C, 1 h). Left: concentration-dependent labeling with (*R*,*R*)-**22**. Right: competition labeling by PF-00835231, (*R*,*R*)-**18**, and Jun8-76-3A. The red arrow indicates the fluorescence band of SARS-CoV-2 M^{pro}. (D) Proteome-wide reactivity profile of **22** and acrylamide probe **23** in live A431 cells (37 °C, 1 h).

Conclusions

In summary, we have developed a novel irreversible inhibitor of SARS-CoV-2 M^{pro} using CFA as a reactive warhead. The convenient synthesis by Ugi MCR facilitated the rapid SAR study to identify the dipeptidic CFA compound **18** and **19** as potent M^{pro} inhibitors. Careful analysis of the diastereoselective inhibition of **18** and establishment of the synthetic protocol for enantiopure CFA derivatives revealed that (*R*,*R*)-**18** exclusively shows strong inhibitory activity among the stereoisomers. The detailed reaction kinetics and computational studies suggest that the fluorine atom of the CFA warhead could participate in the reaction by forming an NH···F hydrogen bond in the M^{pro} active site that induces the stereoselective activation of (*R*,*R*)-**18** for covalent modification. This reaction activation represents another possible utility of the CFA warhead, achievable by the unique characteristics of fluorine atoms, such as the solid electron-withdrawing ability.[39,40] We believe that the prominent role of the CFA chirality in cysteine conjugation would provide an additional opportunity for the improvement of potency and selectivity of covalent inhibitors. Further application of the CFA chirality to the selective inhibition of other disease-associated proteins is ongoing and will be reported in due course.

Data availability

Additional figures as described in the text, experimental procedures, synthetic procedures, and spectral data of the target compounds are available in the ESI.† Crystallographic data for **21B** and **18B** have been deposited in the Cambridge Crystallographic Data Centre (CCDC) under accession numbers CCDC 2124399 and 2124400, respectively.

Author contributions

N. S. and A. O. conceived the project and designed the experiments. N. S., D. Y., S. O., H. I., R. H., T. H., and E. K. synthesized the compounds. N. S., D. Y., and S. O. performed enzymatic experiments. S. R. and K. M. carried out computational experiments. N. S. and A. O. wrote the manuscript with inputs from all authors.

Conflicts of interest

There are no conflicts to declare.

Acknowledgements

This work was supported by Grant-in-Aid for Scientific Research on Innovative Areas "Chemistry for Multimolecular Crowding Biosystems" (JSPS KAKENHI Grant No. JP17H06349) and Platform Project for Supporting Drug Discovery and Life Science Research (Basis for Supporting Innovative Drug Discovery and Life Science Research (BINDS)) from AMED under Grant Number JP18am0101091. N. S. acknowledges Grant-in-Aid for Scientific Research B (JSPS KAKENHI Grant No. 19H02854),

AMED under Grant Number JP21ak0101121, and Grant for Basic Science Research Projects from the Sumitomo Foundation, for their financial supports. A. O. acknowledges AMED under Grant Number JP20fk0108519. We thank Dr Taisuke Matsumoto (Institute for Materials Chemistry and Engineering, Kyushu University) for X-ray diffraction experiments.

Notes and references

1 F. Wu, S. Zhao, B. Yu, Y.-M. Chen, W. Wang, Z.-G. Song, Y. Hu, Z.-W. Tao, J.-H. Tian, Y.-Y. Pei, M.-L. Yuan, Y.-L. Zhang, F.-H. Dai, Y. Liu, Q.-M. Wang, J.-J. Zheng, L. Xu, E. C. Holmes and Y.-Z. Zhang, *Nature*, 2020, **579**, 265–269.

2 P. Zhou, X.-L. Yang, X.-G. Wang, B. Hu, L. Zhang, W. Zhang, H.-R. Si, Y. Zhu, B. Li, C.-L. Huang, H.-D. Chen, J. Chen, Y. Luo, H. Guo, R.-D. Jiang, M.-Q. Liu, Y. Chen, X.-R. Shen, X. Wang, X.-S. Zheng, K. Zhao, Q.-J. Chen, F. Deng, L.-L. Liu, B. Yan, F.-X. Zhan, Y.-Y. Wang, G.-F. Xiao and Z.-L. Shi, *Nature*, 2020, **579**, 270–273.

3 W. T. Harvey, A. M. Carabelli, B. Jackson, R. K. Gupta, E. C. Thomson, E. M. Harrison, C. Ludden, R. Reeve, A. Rambaut, C. G. U. Consortium, S. J. Peacock and D. L. Robertson, *Nat. Rev. Microbiol.*, 2021, **19**, 409–424.

4 C. Gil, T. Ginex, I. Maestro, V. Nozal, L. Barrado-Gil, M. Á. Cuesta-Geijo, J. Urquiza, D. Ramírez, C. Alonso, N. E. Campillo and A. Martinez, *J. Med. Chem.*, 2020, **63**, 12359–12386.

5 T. Pillaiyar, S. Meenakshisundaram and M. Manickam, *Drug Discovery Today*, 2020, **25**, 668–688.

6 R. Cannalire, C. Cerchia, A. R. Beccari, F. S. Di Leva and V. Summa, *J. Med. Chem.*, 2020, DOI: 10.1021/acs.jmedchem.0c01140.

7 Z. Jin, X. Du, Y. Xu, Y. Deng, M. Liu, Y. Zhao, B. Zhang, X. Li, L. Zhang, C. Peng, Y. Duan, J. Yu, L. Wang, K. Yang, F. Liu, R. Jiang, X. Yang, T. You, X. Liu, X. Yang, F. Bai, H. Liu, X. Liu, L. W. Guddat, W. Xu, G. Xiao, C. Qin, Z. Shi, H. Jiang, Z. Rao and H. Yang, *Nature*, 2020, **582**, 289–293.

8 W. Rut, K. Groborz, L. Zhang, X. Sun, M. Zmudzinski, B. Pawlik, X. Wang, D. Jochmans, J. Neyts, W. Młynarski, R. Hilgenfeld and M. Drag, *Nat. Chem. Biol.*, 2021, **17**, 222–228.

9 K. Anand, J. Ziebuhr, P. Wadhwani, J. R. Mesters and R. Hilgenfeld, *Science*, 2003, **300**, 1763–1767.

10 A. Wu, Y. Wang, C. Zeng, X. Huang, S. Xu, C. Su, M. Wang, Y. Chen and D. Guo, *Virus Res.*, 2015, **208**, 56–65.

11 L. Zhang, D. Lin, X. Sun, U. Curth, C. Drosten, L. Sauerhering, S. Becker, K. Rox and R. Hilgenfeld, *Science*, 2020, **368**, 409–412.

12 W. Dai, B. Zhang, X.-M. Jiang, H. Su, J. Li, Y. Zhao, X. Xie, Z. Jin, J. Peng, F. Liu, C. Li, Y. Li, F. Bai, H. Wang, X. Cheng, X. Cen, S. Hu, X. Yang, J. Wang, X. Liu, G. Xiao, H. Jiang, Z. Rao, L.-K. Zhang, Y. Xu, H. Yang and H. Liu, *Science*, 2020, **368**, 1331–1335.

13 J. Qiao, Y.-S. Li, R. Zeng, F.-L. Liu, R.-H. Luo, C. Huang, Y.-F. Wang, J. Zhang, B. Quan, C. Shen, X. Mao, X. Liu, W. Sun, W. Yang, X. Ni, K. Wang, L. Xu, Z.-L. Duan, Q.-C. Zou, H.-L. Zhang, W. Qu, Y.-H.-P. Long, M.-H. Li, R.-C. Yang, X. Liu, J. You, Y. Zhou, R. Yao, W.-P. Li, J.-M. Liu, P. Chen, Y. Liu, G.-F. Lin, X. Yang, J. Zou, L. Li, Y. Hu, G.-W. Lu, W.-M. Li, Y.-Q. Wei, Y.-T. Zheng, J. Lei and S. Yang, *Science*, 2021, **371**, 1374–1378.

14 K. S. Yang, X. R. Ma, Y. Ma, Y. R. Alugubelli, D. A. Scott, E. C. Vatansever, A. K. Drelich, B. Sankaran, Z. Z. Geng, L. R. Blankenship, H. E. Ward, Y. J. Sheng, J. C. Hsu, K. C. K. B. Zhao, H. S. Hayatshahi, J. Liu, P. Li, C. A. Fierke, C.-T. K. Tseng, S. Xu and W. R. Liu, *ChemMedChem*, 2021, **16**, 942–948.

15 W. Dai, D. Jochmans, H. Xie, H. Yang, J. Li, H. Su, D. Chang, J. Wang, J. Peng, L. Zhu, Y. Nian, R. Hilgenfeld, H. Jiang, K. Chen, L. Zhang, Y. Xu, J. Neyts and H. Liu, *J. Med. Chem.*, 2021, DOI: 10.1021/acs.jmedchem.0c02258.

16 R. L. Hoffman, R. S. Kania, M. A. Brothers, J. F. Davies, R. A. Ferre, K. S. Gajiwala, M. He, R. J. Hogan, K. Kozminski, L. Y. Li, J. W. Lockner, J. Lou, M. T. Marra, L. J. Mitchell, B. W. Murray, J. A. Nieman, S. Noell, S. P. Planken, T. Rowe, K. Ryan, G. J. Smith, J. E. Solowiej, C. M. Steppan and B. Taggart, *J. Med. Chem.*, 2020, **63**, 12725–12747.

17 S. Hattori, N. Higashi-Kuwata, H. Hayashi, S. R. Allu, J. Raghavaiah, H. Bulut, D. Das, B. J. Anson, E. K. Lendy, Y. Takamatsu, N. Takamune, N. Kishimoto, K. Murayama, K. Hasegawa, M. Li, D. A. Davis, E. N. Kodama, R. Yarchoan, A. Wlodawer, S. Misumi, A. D. Mesecar, A. K. Ghosh and H. Mitsuya, *Nat. Commun.*, 2021, **12**, 668.

18 B. Bai, A. Belovodskiy, M. Hena, A. S. Kandadai, M. A. Joyce, H. A. Saffran, J. A. Shields, M. B. Khan, E. Arutyunova, J. Lu, S. K. Bajwa, D. Hockman, C. Fischer, T. Lamer, W. Vuong, M. J. van Belkum, Z. Gu, F. Lin, Y. Du, J. Xu, M. Rahim, H. S. Young, J. C. Vederas, D. L. Tyrrell, M. J. Lemieux and J. A. Nieman, *J. Med. Chem.*, 2021, DOI: 10.1021/acs.jmedchem.1c00616.

19 S. Konno, K. Kobayashi, M. Senda, Y. Funai, Y. Seki, I. Tamai, L. Schäkel, K. Sakata, T. Pillaiyar, A. Taguchi, A. Taniguchi, M. Gütschow, C. E. Müller, K. Takeuchi, M. Hirohama, A. Kawaguchi, M. Kojima, T. Senda, Y. Shirasaka, W. Kamitani and Y. Hayashi, *J. Med. Chem.*, 2021, DOI: 10.1021/acs.jmedchem.1c00665.

20 J. Breidenbach, C. Lemke, T. Pillaiyar, L. Schäkel, G. Al Hamwi, M. Diett, R. Gedschold, N. Geiger, V. Lopez, S. Mirza, V. Namasivayam, A. C. Schiedel, K. Sylvester, D. Thimm, C. Vielmuth, L. P. Vu, M. Zyulina, J. Bodem, M. Gütschow and C. E. Müller, *Angew. Chem., Int. Ed.*, 2021, **60**, 10423–10429.

21 D. R. Owen, C. M. N. Allerton, A. S. Anderson, L. Aschenbrenner, M. Avery, S. Berritt, B. Boras, R. D. Cardin, A. Carlo, K. J. Coffman, A. Dantonio, L. Di, H. Eng, R. Ferre, K. S. Gajiwala, S. A. Gibson, S. E. Greasley, B. L. Hurst, E. P. Kadar, A. S. Kalgutkar, J. C. Lee, J. Lee, W. Liu, S. W. Mason, S. Noell, J. J. Novak, R. S. Obach, K. Ogilvie, N. C. Patel, M. Pettersson, D. K. Rai, M. R. Reese, M. F. Sammons, J. G. Sathish, R. S. P. Singh, C. M. Steppan, A. E. Stewart, J. B. Tuttle,

L. Updyke, P. R. Verhoest, L. Wei, Q. Yang and Y. Zhu, *Science*, 2021, **374**, 1586–1593.

22 J. Jacobs, V. Grum-Tokars, Y. Zhou, M. Turlington, S. A. Saldanha, P. Chase, A. Eggler, E. S. Dawson, Y. M. Baez-Santos, S. Tomar, A. M. Mielech, S. C. Baker, C. W. Lindsley, P. Hodder, A. Mesecar and S. R. Stauffer, *J. Med. Chem.*, 2013, **56**, 534–546.

23 N. Kitamura, M. D. Sacco, C. Ma, Y. Hu, J. A. Townsend, X. Meng, F. Zhang, X. Zhang, M. Ba, T. Szeto, A. Kukuljac, M. T. Marty, D. Schultz, S. Cherry, Y. Xiang, Y. Chen and J. Wang, *J. Med. Chem.*, 2021, DOI: 10.1021/acs.jmedchem.1c00509.

24 D. Zaidman, P. Gehrtz, M. Filep, D. Fearon, R. Gabizon, A. Douangamath, J. Prilusky, S. Duberstein, G. Cohen, C. D. Owen, E. Resnick, C. Strain-Damerell, P. Lukacik, C.-M. Consortium, H. Barr, M. A. Walsh, F. von Delft and N. London, *Cell Chem. Biol.*, 2021, **28**, 1795–1806.

25 J. Singh, R. C. Petter, T. A. Baillie and A. Whitty, *Nat. Rev. Drug Discov*, 2011, **10**, 307–317.

26 F. M. Ferguson and N. S. Gray, *Nat. Rev. Drug Discovery*, 2018, **17**, 353–377.

27 D. Kim, J. Y. Xue and P. Lito, *Cell*, 2020, **183**, 850–859.

28 U. P. Dahal, R. S. Obach and A. M. Gilbert, *Chem. Res. Toxicol.*, 2013, **26**, 1739–1745.

29 N. Shindo, H. Fuchida, M. Sato, K. Watari, T. Shibata, K. Kuwata, C. Miura, K. Okamoto, Y. Hatsuyama, K. Tokunaga, S. Sakamoto, S. Morimoto, Y. Abe, M. Shiroishi, J. M. M. Caaveiro, T. Ueda, T. Tamura, N. Matsunaga, T. Nakao, S. Koyanagi, S. Ohdo, Y. Yamaguchi, I. Hamachi, M. Ono and A. Ojida, *Nat. Chem. Biol.*, 2019, **15**, 250–258.

30 M. Sato, H. Fuchida, N. Shindo, K. Kuwata, K. Tokunaga, X.-L. Guo, R. Inamori, K. Hosokawa, K. Watari, T. Shibata, N. Matsunaga, S. Koyanagi, S. Ohdo, M. Ono and A. Ojida, *ACS Med. Chem. Lett.*, 2020, **11**, 1137–1144.

31 C. Miura, N. Shindo, K. Okamoto, K. Kuwata and A. Ojida, *Chem. Pharm. Bull.*, 2020, **68**, 1074–1081.

32 C.-J. Kuo, Y.-H. Chi, J. T.-A. Hsu and P.-H. Liang, *Biochem. Biophys. Res. Commun.*, 2004, **318**, 862–867.

33 M. F. Sowaileh, R. A. Hazlitt and D. A. Colby, *ChemMedChem*, 2017, **12**, 1481–1490.

34 G. Bellucci, G. Berti, A. Borraccini and F. Macchia, *Tetrahedron*, 1969, **25**, 2979–2985.

35 H. Molines and C. Wakselman, *Synthesis*, 1984, **1984**, 838–839.

36 P. J. Tonge, *ACS Infect. Dis.*, 2019, **5**, 796–808.

37 J. Lee, L. J. Worrall, M. Vuckovic, F. I. Rosell, F. Gentile, A.-T. Ton, N. A. Caveney, F. Ban, A. Cherkasov, M. Paetzel and N. C. Strynadka, *Nat. Commun.*, 2020, **11**, 5877.

38 A Ugi MCR-generated dipeptide inhibitor of SARS-CoV-2 M^{pro} with dichloroacetamide warhead (Jun9-62-2R) has been reported while this manuscript was under review. However, none of their active compounds possessed a warhead with chirality at the reaction center, C. Ma, Z. Xia, M. D. Sacco, Y. Hu, J. A. Townsend, X. Meng, J. Choza, H. Tan, J. Jang, M. V. Gongora, X. Zhang, F. Zhang, Y. Xiang, M. T. Marty, Y. Chen and J. Wang, *J. Am. Chem. Soc.*, 2021, **143**, 20697–20709.

39 D. O'Hagan, *Chem. Soc. Rev.*, 2008, **37**, 308–319.

40 P. Zhou, J. Zhou, F. Tian and Z. Shang, *J. Chem. Inf. Model.*, 2009, **49**, 2344–2355.